SolarPACES 2022, 28th International Conference on Concentrating Solar Power and Chemical Energy Systems
Solar Fuels and Chemical Commodities
https://doi.org/10.52825/solarpaces.v1i.647

Published: 27 Mar. 2024

Model-based Predictive Control of a Solar Reactor

Youssef Karout[1,2], Axel Curcio[1,3], Julien Eynard[1,2][https://orcid.org/0000-0002-8011-1098], Stéphane Thil[1,2][https://orcid.org/0000-0002-2609-0687], Sylvain Rodat[3][https://orcid.org/ 0000-0001-6181-0670], Stéphane Abanades[3][https://orcid.org/0000-0002-6689-3652], and Stéphane Grieu[1,2][https://orcid.org/0000-0002-2000-3001]

[1] PROMES-CNRS (UPR 8521), rambla de la thermodynamique, Tecnosud, 66100 Perpignan, France

[2] University Perpignan Via Domitia (UPVD), 52 avenue Paul Alduy, 66860 Perpignan, France

[3] PROMES-CNRS (UPR 8521), 7 rue du four solaire, 66120 Font-Romeu-Odeillo-Via, France

Parts of this paper were published as journal article
Karout, Y.; Curcio, A.; Eynard, J.; Thil, S.; Rodat, S.; Abanades, S.; Vuillerme, V.; Grieu, S. Model-Based Predictive Control of a Solar Hybrid Thermochemical Reactor for High-Temperature Steam Gasification of Biomass. *Clean Technol.* **2023**, *5*, 329-351.
https://doi.org/10.3390/cleantechnol5010018

Abstract. The present paper deals with the modelling and control of a solar reactor designed to produce syngas, by exploiting concentrated solar power. A model of the reactor based on the thermodynamic equilibrium is developed. Two model-based predictive control strategies are proposed: the first strategy (MPC strategy 1) aims to maintain the reactor's temperature at its nominal value whereas the second strategy (MPC strategy 2) aims to maintain the reactor's temperature at its nominal value, while maximizing the use of solar energy. Finally, these strategies are compared to a reference strategy, which is based on a combination of a rule-based controller and an adaptive PID controller with optimized gains. The robustness of the MPC controller to forecast errors is also studied by testing different DNI forecasting models.

Keywords: Model-Based Predictive Control, Solar Reactor, Syngas Production

1. Introduction

The presented work explores the modelling and dynamic control of a solar thermochemical reactor dedicated to the high-temperature steam-gasification of biomass (see Figure 1). Solar gasifiers have been experimentally studied since the early 80s, with the works of Gregg et al. [1] and Taylor et al. [2] about packed-bed and fluidized-bed technologies. Interest in solar thermochemistry has grown with climate-change considerations [3], especially since the mid-2000, leading to major innovative design investigations, as reviewed in Puig-Arnavat et al. [4]. More recent works have been proposed about double-loop fluidized beds, to separate oxidation and reduction zones for thermodynamic-cycle-based operation [5], or to separate gasification and combustion zones for a solar-autothermal hybrid operation [6]. A solar spouted-bed gasifier was conceived by Bellouard et al. [7], and its hybrid solar-autothermal operation was investigated successively by Boujjat et al. [8] and Curcio et al. [9] (see Figure 1). Other recent experimental works have demonstrated the feasibility of such hybrid operation [10], [11], but the question of its dynamic control is still open. It should be mentioned that the laboratory PROMES possesses a solar reactor prototype, designed with the help of the CEA-LITEN, in order to contribute to the WP8 of the SFERA project. Thus, a dynamic controller is developed, using image-based DNI forecasts inspired from the first part of this thesis, to maintain the performance and stability of the solar reactor. To be able to achieve this task, a reactor model

is required. This model is provided following the collaboration between PROMES-CNRS and CEA-LITEN [8], [12]. The present work aims at conciliating the solar-autothermal hybrid control strategy of a gasifier with the efficient implementation of an MPC algorithm. Several strategies can be developed, such as the maximizing syngas production, maintaining reactor's stability, etc. However, in this work and based on the developed reactor model, the goal is to maintain reactor's stability to ensure optimal conditions for the chemical reactions taking place in the reactor. The MPC controller acts on the oxygen flow and the mirrors' defocussing factor, in order to maintain the nominal temperature of the reactor, ensuring its stability. At this level, two MPC strategies are proposed: first strategy aims to maintain the reactor temperature at any cost; the second strategy aims to maintain the reactor temperature while minimizing the oxygen consumption in the process. This controller is then compared to an adaptive PID controller with optimized gains to highlight the amelioration brought by MPC. Furthermore, the MPC controller is implemented with different forecasts: perfect forecasts, smart persistence forecasts, and forecasts provided by a sky-imaging-based model. Also, a study is carried out to discuss the effect of forecast errors on the MPC's performance.

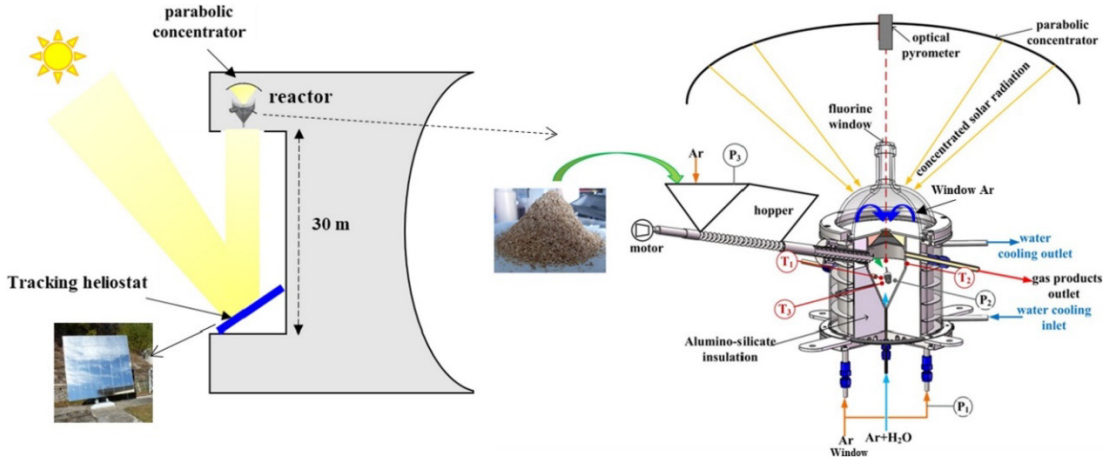

Figure 1. Solar reactor design.

2. Modelling of the solar reactor

The model is inspired by the work of Boujjat et al. [12], who computed the production of a solar biomass gasifier over one year to assess its allothermal-autothermal hybridization. The gasifier is designed to be heated by both concentrated solar power (allothermal heating) and in-situ combustion (autothermal heating) [7], [8], enabling a continuous conversion of biomass around the clock. For a biomass flow rate maintained constant at 1.465 t h^{-1}, the reactor parameters are set so that the nominal temperature of 1473 K (1199.85 °C) is reached for a DNI equal to 800 W m^{-2}, which corresponds to around 80% of the maximum DNI obtained during a year. At thermodynamic equilibrium, the chemical reactions taking place in the solar reactor are modelled as follows:

- When DNI is higher than 800 W m^{-2} and the reactor's temperature is at its nominal value, only the endothermic reaction of gasification occurs, as described by the following equation:

$$CH_{1.66}O_{0.69} + 0.31\ H_2O \rightarrow CO + 1.14\ H_2 \quad (1)$$

- When DNI is lower than 800 W m^{-2} and the reactor's temperature is lower than its nominal value, the injection of oxygen is necessary to maintain the reactor temperature at its steady state level. The impact of oxygen injection can be described by, as a first approximation, the oxy-combustion of wood:

$$CH_{1.66}O_{0.69} + 1.07\ O_2 \rightarrow CO_2 + 0.83\ H_2 \quad (2)$$

The model also includes the thermal balance of the reactor walls, and a thermodynamic calculation coded with the open-source library CANTERA [13]:

$$Q_{Sun} = D \cdot C \cdot \eta_{optical} \cdot A_{aperture} \cdot DNI \quad (3)$$

$$Q_{radiationloss} = \sigma \cdot A_{aperture} \cdot \left(T^4 - T_{amb}^4\right) \quad (4)$$

$$Q_{conductionloss} = (T - T_{amb})/R \quad (5)$$

$$Q_{reaction} = \sum_{i=1}^{n_{rea}} f_i^{in} h_i(T_{amb}) - \sum_{i=1}^{n_{prod}} f_i^{out} h_i(T) \quad (6)$$

where h_i is the enthalpy of reactants and products, f_i^{in} and f_i^{out} are the flow rates of reactants and products, respectively, n_{rea} and n_{prod} are the number of reactants and products, respectively, D is the defocussing factor, $Q_{reaction}$ is the power gained from the chemical reaction, Q_{Sun} is the power obtained from the Sun, $Q_{radiationloss}$ is the power lost by radiation, $Q_{conductionloss}$ is the power lost by conduction, m is the mass of the reactor walls, $C_{p,w}$ is the specific heat of the reactor walls, C is th concentration factor, $\eta_{optical}$ is th optical efficiency, $A_{aperture}$ is the aperture's area, σ is the Stefan-Boltzmann constant, T_{amb} is the ambient temperature, and R is the conduction thermal resistance.

The reactor's temperature can be modeled through the following first-order nonlinear ordinary differential equation (Equation 7) which represents the heat balance of the reactor:

$$m \cdot C_{p,w} \cdot \frac{dT}{dt} = Q_{reaction}\left(f_{steam}^{in}, f_{biomass}^{in}, f_{oxygen}^{in}, T\right) + Q_{net} \quad (7)$$

$$Q_{net} = Q_{Sun} - Q_{radiationloss} - Q_{conductionloss} \quad (8)$$

where Q_{net} is the power resulting from the solar power gained and the power lost due to the radiation and conduction losses (Equation 8).

Above a DNI value of 800 W m^{-2}, a reduction of the input solar power is necessary to maintain the reactor's temperature at 1473 K. As a result, a defocussing factor *D* is introduced (Equation 3). Below this DNI value, oxygen is added to heat the reactor thanks to in-situ combustion, which directly alters the syngas composition by shifting the thermodynamic equilibrium. Finally, when DNI is lower than 150 W m^{-2}, the reactor's aperture is closed to limit the radiation loss.

3. Development of control strategies for the solar reactor

This section starts with the development of a reference controller, which is a combination of a rule-based controller and an adaptive PID controller with optimized gains. Then, the proposed MPC strategies (MPC strategy 1 and MPC strategy 2) are presented by explaining the different optimization problems, the corresponding constraints, and the developed DNI forecast model. These controllers are then evaluated in the following sections. For the control of the solar reactor, the discretized reactor model $\mathcal{M}$ is represented as follows:

$$T(t+1) = \mathcal{M}\left(D(t), f_{oxygen}^{in}, T(t)\right) \quad (9)$$

In the sequel, the biomass flow rate $f_{biomass}^{in}$ and the steam flow rate f_{steam}^{in} are fixed to their nominal design values of 1.465 t h^{-1} and 0.26 t h^{-1}, respectively.

3.1 Reference controller

The goal of this controller is to maintain the temperature inside the reactor at its nominal value (1473 K) to ensure its stability. This controller is developed in order to have a reference to which the MPC controller can be compared.

The control variables are:

- the oxygen flow rate (f_{oxygen}^{in}): in case of a DNI deficit (800 W m^{-2}), oxygen can be injected to increase the reactor's temperature by burning biomass, it is controlled by an adaptive PID controller with optimized gains, where for each of the three intervals of DNI values, the gains (K_p, K_i and K_d) have been obtained by solving an optimization problem (see Table 1).
- the defocussing factor (D): in case of an excess of DNI (DNI > 800 W m^{-2}), the mirrors can be defocussed to compensate for the surplus. The mirrors' defocussing factor is controlled as follows:

$$D(t) = \begin{cases} 1 \text{ if } DNI(t) \leq 800\ Wm^{-2} \text{ and } T(t) < 1473K \\ \dfrac{800}{DNI(t)} \text{ if } DNI(t) > 800\ Wm^{-2} \text{ and } T(t) > 1473K \end{cases} \quad (10)$$

Table 1. Optimized gains of the adaptive PID controller.

Gain	DNI < 150 W m^{-2}	150 W m^{-2} < DNI < 800 W m^{-2}	DNI > 800 W m^{-2}
K_p	1.6 x 10^{-2}	3.4 x 10^{-2}	1.5 x 10^{-3}
K_i	0	9 x 10^{-4}	1.5 x 10^{-4}
K_d	1.2 x 10^{-2}	2.5 x 10^{-2}	1 x 10^{-5}

3.2 Model-based predictive control of the solar reactor

In this section, the two MPC strategies are detailed: two optimization problems are considered, and the developed approach to forecast DNI is briefly explained. The MPC strategy 1 aims to maintain the reactor's temperature without considering the oxygen consumption whereas and the MPC strategy 2 aims to maintain the reactor's temperature while exploiting the solar energy and minimizing the oxygen consumption. Let n be the number of time steps in the prediction horizon of the controller. At each of those n time steps, an optimization problem is solved to find optimal inputs $\boldsymbol{D} \in R^n$ and $\boldsymbol{f}_{oxygen}$ [14], for a given objective function, a set of constrains, and bounds. This optimization problem thus defines the control strategy. In this paper, two strategies are presented. The first strategy (i.e., MPC strategy 1) is about solving the following optimization problem at instant t:

$$\left(D^*, f_{oxygen}^{in\,*}\right) = \text{argmin} \sum_{k=1}^{n} \left(S_p - T(t+k)\right)^2 \quad (11)$$

where: $\boldsymbol{T(t+1) = \mathcal{M}\left(D(t), f_{oxygen}^{in}, T(t)\right)}$, $\boldsymbol{0 \leq D(t+k) \leq 1}$ and $\boldsymbol{0 \leq f_{oxygen}^{in}(t+k) \leq 2}$.

It focuses on minimizing the squared difference between the temperature setpoint and the simulated temperature over the considered prediction horizon, without constraints on the oxygen consumption or the usage of solar energy. The second strategy (i.e., MPC strategy 2) is about solving the following optimization problem at instant t:

$$\left(D^*, f_{oxygen}^{in\,*}\right) = \text{argmin} \sum_{k=1}^{n} \alpha \left(S_p - T(t+k)\right)^2 + \beta \left(f_{oxygen}^{in}(t+k)\right)^2 - \gamma\left(D(t+k)\right)^2 \quad (12)$$

where: $\boldsymbol{T(t+1) = \mathcal{M}\left(D(t), f_{oxygen}^{in}, T(t)\right)}$, $\boldsymbol{0 \leq D(t+k) \leq 1}$ and $\boldsymbol{0 \leq f_{oxygen}^{in}(t+k) \leq 2}$.

As can be seen, the goal is here to make a trade-off between following the temperature setpoint, minimizing the oxygen consumption, and maximizing the use of solar energy. This

trade-off is determined by the weights α, β, and γ. It should be noted that DNI forecasts are needed to solve these optimization problems. How these forecasts are obtained is the subject of the following section. DNI forecasts must be provided to the MPC controller for every time step in its prediction horizon. Three types of forecasts are considered in this study to evaluate the robustness of the MPC controller to forecast errors: perfect forecasts, smart persistence forecasts, and image-based forecasts. The proposed image-based forecasting model relies on the hybridization between the smart persistence model and a recurrent neural network (RNN) model. It processes high dynamic range (HDR) images, provided by a sky imager, to forecast sudden DNI variations.

4. Evaluation of the control strategies

The controllers' performance is evaluated by calculating the root mean squared error (RMSE), the oxygen consumption, and the average temperature variation (ATV), which estimates the magnitude of temperature variation inside the reactor (except for DNI < 150 W m^{-2}, since in this case the reactor is closed and there is no power loss; the temperature can thus be easily maintained by injecting 0.88 t h^{-1}. This study is made over a 7-day test dataset. It should be mentioned that night-time periods are not included, since they are identical to the case with DNI < 150 W m^{-2} where injecting 0.88 t h^{-1} is sufficient to maintain perfectly the reactor's temperature. The control inputs, for both MPC strategies, are initialized as follows:

- $D(t+k) = 1 \; \forall k \in [\![1; n]\!]$. This initialization is chosen so that the optimal input found is near 1, which means that the use of solar energy is maximized;
- $f_{oxygen}^{in}(t+k) = 0.5 \; \forall k \in [\![1; n]\!]$. This initialization is chosen to ensure that the optimizer converges fast to the optimal solution, which is around 0.5 t h^{-1}. Other initialization values resulted in an increase in computation time and some performance degradation.

In this work, the trust-region constrained algorithm [15] is used, for its ability to solve non-linear optimization problems and its high robustness and its ability to handle various objective functions. After the optimization of the prediction horizon, the MPC implementation results, presented in Table 2, over one week show that the MPC controller is able to maintain the reactor's temperature (MPC strategy 1) and to exploit the solar power by minimizing oxygen consumption (MPC strategy 2). Furthermore, the integration of image-based forecasts results in better performance for both strategies: the MPC controller with image-based forecasts scores lower RMSE values (around 7.5%) and lower oxygen consumption (saving up to 1000 kg of oxygen) (MPC strategy 1) and scores lower RMSE values (around 6.4%) for an increase in oxygen consumption of less than 0.1% (MPC strategy 2).

Table 2. Comparison between the two proposed MPC strategies with optimal prediction horizon. For MPC strategy 1, the optimal prediction horizon is 2 min for all forecasting models. For MPC strategy 2, the optimal prediction horizons are 1 min (perfect forecasts), 1.5 min (smart persistence forecasts) and 2 min (image-based forecasts). Reference strategy: RMSE is 4.88 K, oxygen consumption is 31 933 kg, and ATV is 2.27 K.

Strategy	Performance criterion	Perfect forecasts	Image-based forecasts	Smart persistence forecasts
MPC strategy 1	RMSE [K] O_2 cons. [kg] ATV [K]	$\ll 0.01$ 41 920.00 $\ll 0.01$	1.34 36 365.80 1.32	1.45 38 509.00 1.32
MPC strategy 2	RMSE [K] O_2 cons. [kg] ATV [K]	0.07 31 968.33 0.03	1.60 32 091.00 1.54	1.71 32 089.23 1.54

In addition, the MPC controller, with all forecast models, manages to outperform the reference controller by scoring lower RMSE and ATV values at the cost of an increase in

oxygen consumption of less than 11% (MPC strategy 1) and less than 0.5% (MPC strategy 2). This analysis ensures the robustness of the MPC controller to forecasts errors and proves the feasibility of the approach. The two proposed MPC strategies have their advantages and disadvantages. Table 2 presents the performance of the MPC controller (MPC strategies 1 and 2) with the optimal prediction horizon. When perfect forecasts are provided, the MPC strategy 2 is considered a better approach since the reference tracking error increase is minimal compared to the amount of saved oxygen (around 24%). However, when forecasts are provided by the smart persistence model or the proposed image-based model, the first strategy (MPC strategy 1) is better if low RMSE and ATV values are required, since this strategy scores around 14% lower RMSE than the second strategy (MPC strategy 2; image-based forecasts are used). The second strategy (MPC strategy 2) can be adopted if the oxygen injected should be absolutely minimized, since it can save around 11% of oxygen consumption (image-based forecasts are used).

5. Conclusion

This paper deals with the predictive control of a solar reactor that exploits concentrated solar power to produce syngas. An MPC controller (two strategies) is proposed and compared to a reference controller which consists of a rule-based controller and an adaptive PID controller with optimized gains. These two MPC strategies target different performances: the first strategy (i.e., MPC strategy 1) focuses on preserving the reactor's stability by maintaining its nominal temperature; the second strategy (i.e., MPC strategy 2) finds a trade-off between maintaining the reactor's temperature and minimizing the oxygen consumption while exploiting solar energy. This study can then be extended to more complicated strategies like, maximization of the syngas production, however, this would necessitate a model adapted for this study. Different DNI forecasts are provided to the MPC controller: perfect forecasts, which produce optimal performance; smart persistence forecasts, which produce reference performance; image-based forecasts, where the model processes HDR sky images to forecasts DNI by predicting possible DNI variations. This study is carried out to showcase the robustness of the controller to forecast errors. Results of the MPC implementation show that the MPC controller is able to maintain the reactor's temperature (MPC strategy 1) and to exploit the solar power by minimizing oxygen consumption (MPC strategy 2). Furthermore, the integration of image-based forecasts results in better performance for both strategies.

Data availability statement

The data presented in this study are available on request from the corresponding author.

Author contributions

The authors contributed equally to this work.

Competing interests

The authors declare that they have no competing interests.

Funding

This research was financially supported by the European Union’s Horizon 2020 research and innovation programme under the grant agreement No. 823802 (Solar Facilities for the European Research Area - Third Phase [SFERA III]) [3].

References

1. D. Gregg et al. Solar gasification of coal, activated carbon, coke and coal and biomass mixtures. In: Solar Energy 25.4 (1980), pp. 353-364. DOI: 10.1016/0038-092x(80)90347-3.
2. R. Taylor et al. Solar gasification of carbonaceous materials. In: Solar Energy 30.6 (1983), pp. 513-525. DOI: 10.1016/0038-092x(83)90063-4.
3. D. Yadav and R. Banerjee. A review of solar thermochemical processes. In: Renewable and Sustainable Energy Reviews 54 (Feb. 2016), pp. 497-532. DOI: 10.1016/j.rser.2015.10.026.
4. M. Puig-Arnavat et al. State of the art on reactor designs for solar gasification of carbonaceous feedstock. In: Solar Energy 97 (Nov. 2013), pp. 67-84. DOI: 10.1016/j.solener.2013.08.001.
5. M. Milanese et al. Modeling of double-loop fluidized bed solar reactor for efficient thermochemical fuel production. In: Solar Energy Materials and Solar Cells 160 (Feb. 2017), pp. 174-181. DOI: 10.1016/j.solmat.2016.10.028.
6. A. Gómez-Barea et al. Analysis of fluidized bed gasification of biomass assisted by solar-heated particles. In: Biomass Conversion and Biorefinery 11.1 (Sept. 2020), pp. 143-158. DOI: 10.1007/s13399-020-00865-0.B.
7. Q. Bellouard et al. Biomass Gasification in an Innovative Spouted-Bed Solar Reactor: Experimental Proof of Concept and Parametric Study. In: Energy Fuels 31.10 (Sept. 2017), pp. 10933-10945. DOI: 10.1021/acs.energyfuels.7b01839.
8. H. Boujjat et al. Experimental and numerical study of a directly irradiated hybrid solar/combustion spouted bed reactor for continuous steam gasification of biomass. In: Energy 189 (Dec. 2019), p. 116118. DOI: 10.1016/j.energy.2019.116118.
9. A. Curcio et al. Experimental assessment of woody biomass gasification in a hybridized solar powered reactor featuring direct and indirect heating modes. In: International Journal of Hydrogen Energy 46.75 (Oct. 2021), pp. 37192-37207. DOI: 10.1016/j.ijhydene.2021.09.008.
10. A. P. Muroyama et al. Design and demonstration of a prototype 1.5 kWth hybrid solar/autothermal steam gasifier. In: Fuel 211 (Jan. 2018), pp. 331-340. DOI: 10.1016/j.fuel.2017.09.059.
11. B. J. Hathaway and J. H. Davidson. Autothermal hybridization and controlled production of hydrogen-rich syngas in a molten salt solar gasifier. In: International Journal of Hydrogen Energy 46.29 (Apr. 2021), pp. 15257–15267. DOI: 10.1016/j.ijhydene.2021.02.048.
12. H. Boujjat et al. Dynamic simulation and control of solar biomass gasification for hydrogen-rich syngas production during allothermal and hybrid solar/autothermal operation. In: International Journal of Hydrogen Energy 45.48 (Sept. 2020), pp. 25827–25837. DOI: 10.1016/j.ijhydene.2020.01.072.
13. D. G. Goodwin et al. Cantera: An Object-oriented Software Toolkit for Chemical Kinetics, Thermodynamics, and Transport Processes. 2021. DOI: 10.5281/ZENODO.4527812.
14. C. E. García et al. Model predictive control: Theory and practice-A survey. In: Automatica 25.3 (May 1989), pp. 335-348. DOI: 10.1016/0005-1098(89)90002-2.
15. A. R. Conn et al. Trust Region Methods. Society for Industrial and Applied Mathematics, Jan. 2000. DOI: 10.1137/1.9780898719857.